Catalysis Today 150 (2010) 119–127

Contents lists available at ScienceDirect

Catalysis Today

journal homepage: www.elsevier.com/locate/cattod

Preparation of highly loaded Pt/carbon xerogel catalysts for Proton Exchange Membrane fuel cells by the Strong Electrostatic Adsorption method

Nathalie Job [a,*], Stéphanie Lambert [a], Marian Chatenet [b], Cédric J. Gommes [a], Frédéric Maillard [b], Sandrine Berthon-Fabry [c], John R. Regalbuto [d], Jean-Paul Pirard [a]

[a] Université de Liège, Laboratoire de Génie Chimique (B6a), B-4000 Liège, Belgium
[b] Laboratoire d'Électrochimie et de Physico-chimie des Matériaux et des Interfaces (LEPMI), UMR 5631 CNRS/Grenoble-INP/UJF, BP75, F-38402 St Martin d'Hères Cedex, France
[c] Mines ParisTech, Centre Énergétique et Procédés, BP 207, F-06904 Sophia-Antipolis Cedex, France
[d] Chemical Engineering Department, University of Illinois, 810 S. Clinton Street, Chicago, IL 60607, USA

ARTICLE INFO

Article history:
Available online 3 August 2009

Keywords:
Carbon xerogels
Pt catalysts
PEM fuel cells

ABSTRACT

Pt/carbon xerogel catalysts were prepared by the Strong Electrostatic Adsorption method: impregnation of the support was performed under optimal conditions, leading to maximum metal weight percentage while keeping the highest possible dispersion. After impregnation with H_2PtCl_6, the samples were filtered, dried and reduced. In order to increase the Pt weight percentage, up to three successive impregnation–drying–reduction cycles were performed. The final metal content of the catalysts was found to increase regularly: 7.5, 15.0 and 22.3 wt.%, after one, two and three cycles, respectively. This indicates that the adsorption sites were fully regenerated after the reduction treatment, and that they were available for the next impregnation step. In each case, the metal particles were found to be highly dispersed (particle size ~2 nm); in addition, the average particle size did not change upon repeated impregnation. The 15.0 wt.% sample was tested as a cathodic catalyst in an H_2/air Proton Exchange Membrane fuel cell: the cathode activity, expressed as a function of the mass of Pt involved, increased up to twice that of previous catalysts prepared by impregnation with H_2PtCl_6 and reduction in aqueous phase by $NaBH_4$, provided the final reduction temperature of the catalyst was increased up to 450 °C.

1. Introduction

The catalytic layers of Proton Exchange Membrane (PEM) fuel cells, usually composed of Pt/carbon black, gas voids and ionomer, are key elements to the cell performance [1]. Carbon blacks, commonly used for the preparation of the catalysts, are formed of primary carbon particles (~20–60 nm) assembled together as agglomerates (1–100 μm) [2]. The packing of these agglomerates, and therefore the pore structure of the catalytic layers, depends on the nature of the carbon black and on the electrode processing. In order to be electrochemically active, the Pt particles must be in contact with the carbon support and connected to the membrane *via* an ionomer network (Nafion®). In addition, reactants and products should be able to circulate easily through the catalytic layers: (i) the catalyst must be accessible to the gas reactant, through the percolating porous structure of the catalytic layer; (ii) protons and electrons need to be collected by the ionomer and the catalyst support, respectively, and driven to/from the membrane (protons) and the current collector (electrons). Typically, at the air-fed cathode, where the transport of oxygen, protons and water are involved in the oxygen reduction reaction (ORR), high potential losses due to diffusional limitations offset the cell performance.

These diffusional limitations, as well as the sluggish rate of the ORR, are generally compensated by the use of catalytic layers with a high Pt content, which increases the cost of electrodes. According to Gasteiger et al. [3], the mandatory cost reduction could be led *via*: (i) the improvement of the catalyst activity, either by optimizing the metal dispersion or by using appropriate metal alloys, and (ii) the improvement of the catalyst's effectiveness through the development of new catalytic layer structures in order to decrease the diffusion-induced potential losses. In the latter field, *i.e.* the decreasing of diffusional limitations, nanostructured synthetic carbons with controlled pore size and composition, such as carbon xerogels and aerogels, constitute an interesting alternative to carbon blacks [4–6]. Indeed, these carbon materials are synthetic carbons obtained by the drying and pyrolysis of resorcinol–formaldehyde aqueous gels, and their pore texture can be tailored depending on the final application [7–9]. By modifying the synthesis and drying conditions, the pore size and pore volume can be adjusted within a wide range (pore size: ~5 nm to ~3 μm; pore volume: ~0.5 to ~5 $cm^3\ g^{-1}$). In catalysis applications, the flexibility of the pore texture has proved to be a great advantage,

* Corresponding author. Tel.: +32 4366 3537; fax: +32 4366 3545.
E-mail address: Nathalie.Job@ulg.ac.be (N. Job).

0920-5861/$ – see front matter © 2009 Elsevier B.V. All rights reserved.
doi:10.1016/j.cattod.2009.06.022

since diffusional limitations encountered with commercial activated carbons as supports can be decreased or even suppressed [10]. The same effect has been observed in the case of PEM fuel cell cathodes prepared from carbon aerogels [6] and xerogels [5]. However, the Pt/aerogel and Pt/xerogel catalysts used to prepare Membrane-Electrodes Assemblies (MEAs) in previous studies [5,6] did not display a very high Pt dispersion: about 60% of the metal consisted of large Pt particles, which are not interesting in terms of minimizing the cost of the catalytic layers.

In order to increase the Pt dispersion while reaching a high metal content, the so-called 'Strong Electrostatic Adsorption' (SEA) method was used in a previous study to prepare Pt/carbon xerogel catalysts [11]. The SEA method [12] consists of maximizing the electrostatic interactions between the metal precursor and the support by adjusting the pH of the carbon/water/Pt precursor slurry to the adequate value, which depends on both the surface chemistry of the support and the nature of the Pt precursor. In the case of the impregnation of carbon xerogels with H_2PtCl_6 aqueous solutions (1000 ppm_{Pt}), the initial pH leading to the highest Pt uptake was found to be 2.5, and the corresponding maximum Pt weight percentage ranged from 8 to 10 wt.% [11].

However, these weight percentages are not sufficient to allow for good performance of the cathode catalytic layer, while minimizing its thickness, and they need to be increased up to at least 20 wt.%. In addition, a balance between the Pt specific activity (per unit of metal surface area) and the Pt mass activity (per mass unit of metal) is usually reached for Pt particles of a size *ca.* 3–4 nm [13]. Therefore, the aim of this study is to elaborate Pt/carbon xerogel catalysts by the SEA method with: (i) high metal weight percentages (>20 wt.%), (ii) high metal dispersion (particle size ~3–4 nm), and (iii) high electrochemical activity. Since increasing the concentration of Pt precursor in the impregnation solution above 1000 ppm_{Pt} does not lead to an increase in the Pt weight percentage of the final catalyst [11], the impregnation procedure was repeated until about 20 wt.% of Pt was reached.

2. Experimental

2.1. Support and catalyst preparation

The carbon support chosen for this study was a micro-macroporous carbon xerogel with a macropore size ranging from 50 to 85 nm. The material was synthesized by the drying and pyrolysis of a resorcinol–formaldehyde aqueous gel, following a procedure developed in a previous study [9]. The aqueous gel was first obtained by polycondensation of resorcinol (Vel, 99%) with formaldehyde (Aldrich 37 wt.% in water, stabilized with 10–15 wt.% methanol) in water, in the presence of Na_2CO_3 (UCB, 99.5%). The resorcinol/formaldehyde molar ratio, *R*/*F*, was fixed at 0.5, which is usually considered as the stoichiometric ratio [7–9]. The resorcinol/sodium carbonate molar ratio, *R*/*C*, was equal to 1000 while the solvents/(resorcinol + formaldehyde) molar ratio, *D* was chosen equal to 5.7. In *D*, the term 'solvents' includes the deionized water added, and the water and methanol (stabilizer) present in the formaldehyde solution. Gelation and ageing were performed at 85 °C (72 h). The wet material was then dried by evaporation at 60 °C in a vacuum oven, the pressure being reduced from 10^5 to 10^3 Pa over 2 days. The sample was then left at 150 °C and 10^3 Pa for 12 h. Finally, the carbon xerogel was obtained by pyrolysis at 800 °C for 2 h under nitrogen flow [9]. The textural characteristics of the support are shown in Table 1.

Three Pt/C catalysts with different Pt weight percentages were prepared by impregnation with H_2PtCl_6, using the SEA method. The optimal impregnation conditions for carbon xerogels have been determined in a previous study [11]. In brief, the carbon support was first impregnated with an H_2PtCl_6 aqueous solution (4.1 mmol L^{-1}), the pH of which was adjusted to 2.5 with HNO_3 prior to carbon addition. The total material surface area in solution, *i.e.* the surface loading (SL), was fixed at 10^3 m^2 L^{-1}. So, 3.7 g of carbon xerogel (643 m^2 g^{-1}) was mixed with 2.38 L of H_2PtCl_6 solution. After 1 h under magnetic stirring, the slurry was filtrated and the recovered solid was dried in air at 100 °C for 12 h. The catalyst obtained was then reduced under flowing H_2 (0.04 mmol s^{-1}) at 200 °C for 1 h.

Table 1
Textural parameters of the carbon support and catalysts.

Sample	S_{BET} (m^2 g^{-1})	V_{DUB} (cm^3 g^{-1})	V_v (cm^3 g^{-1})	$d_{p,min}$ (nm)	$d_{p,max}$ (nm)
	±5	±0.01	±0.1	±5	±5
Support	643	0.26	2.1	50	85
Catalysts					
X-Pt-1	589	0.24	2.1	50	85
X-Pt-2	577	0.23	2.0	50	85
X-Pt-3	526	0.22	2.0	50	85

S_{BET}: specific surface area determined by the BET method; V_{DUB}: micropore volume obtained by the Dubinin–Radushkevich equation; V_v: total void volume obtained by combination of nitrogen adsorption and mercury porosimetry; $d_{p,min}$: minimum pore size, micropores excluded; $d_{p,max}$: maximum pore size. *Note*: all the parameters are related to the carbon support, metal excluded.

In order to increase the Pt weight percentage, this impregnation–drying–reduction cycle was repeated up to three times using the same original catalyst batch: after one cycle, two-thirds of the catalyst batch were re-impregnated, dried and reduced again under the same conditions. Then, the double-impregnated catalyst was divided into two parts, and one of the fractions was submitted to a third cycle. In the case of the double-impregnated catalyst, a fraction of the sample was reduced at 450 °C for 5 h so as to check for the influence of the reduction conditions on the catalyst properties. Hereafter, the xerogel-supported catalysts are labelled 'X-Pt' followed by the number of impregnation–drying–reduction cycles. So, X-Pt-2 corresponds to a catalyst obtained by double-impregnation of the carbon xerogel support. The catalyst reduced at 450 °C is denoted X-Pt-2/450.

2.2. Physico-chemical characterization of the support and catalysts

The pore texture of the support and final catalysts was characterized by the combination of mercury porosimetry, performed with a Carlo Erba Porosimeter 2000, and nitrogen adsorption–desorption, performed at 77 K with a Sorptomatic Carlo Erba 1900. Hg porosimetry enabled us to obtain the pore volume corresponding to pores of a width >7.5 nm, V_{Hg}. The analysis of the isotherms provided the BET specific surface area, S_{BET}, the micropore volume calculated by the Dubinin–Radushkevich equation, V_{DUB}, and the cumulative volume of pores of a width between 2 and 7.5 nm determined by the Broekhoff–de Boer theory, $V_{cum\,<\,7.5\,nm}$. Since N_2 adsorption–desorption is applicable to the analysis of pores smaller than 50 nm in diameter, and Hg porosimetry is limited to pores larger than 7.5 nm in diameter, the total void volume, V_v, was obtained by combining both techniques [14]:

$$V_v = V_{DUB} + V_{cum<7.5\,nm} + V_{Hg} \quad (1)$$

The metal content of the catalysts after impregnation, drying and reduction was measured by Inductively Coupled Plasma-Atomic Emission Spectrometry (ICP-AES, Iris advantage Thermo Jarrel Ash). The preparation of the Pt solutions from the catalysts is thoroughly described in a previous study [15]. In order to measure the size of the metal particles, the catalysts were investigated by transmission electron microscopy, with a Jeol 2010 (200 kV) device

(LaB_6 filament). The samples were crushed and dispersed in ethanol and subsequently deposited onto a copper grid. Particle size distributions were obtained by image analysis (see Appendix) performed on a set of at least 1000 particles. The metal particles were also analyzed by X-ray diffraction (XRD) with a Siemens D5000 goniometer using the Cu-Kα line (Ni filter). The average metal particle size, d_{XRD}, was estimated using Scherrer's equation [16].

Carbon monoxide chemisorption was used to determine the accessible Pt surface. Briefly, a first CO adsorption isotherm was achieved so as to measure the total amount of adsorbed carbon monoxide (chemisorbed + physisorbed). The catalyst was then outgassed, and a second CO adsorption isotherm was measured in order to evaluate the amount of physisorbed CO. The amount of CO forming the chemisorbed monolayer on surface Pt atoms, $n_{s,m}$, was deduced by subtracting the second isotherm from the first one and extrapolating the nearly horizontal difference curve to the uptake axis. Isotherms were measured with a Fisons Sorptomatic 1990 equipped with a turbomolecular vacuum pump that allows the reaching of a high vacuum of 10^{-3} Pa. The entire procedure, from the sample preparation to the adsorption measurement, is fully described elsewhere [15].

Some samples were analyzed by X-ray photoelectron spectroscopy (XPS). The measurements were carried out on a SSI-X-probe (SSX-100/206) Fisons spectrometer. The samples were fixed to small troughs using double-face adhesive tape and then placed on an insulating homemade ceramic sample holder (Macor, Switzerland). A nickel grid was fixed above the samples, and an electron flood gun was set at 8 eV to compensate for the positive charging of the samples during the analyses. Results are reported in terms of Cl/Pt ratio, calculated from the Cl to Pt peak surface ratio after calibration corrections.

2.3. Fuel cell tests

Two catalysts were tested in PEM fuel cell cathodic catalytic layers in order to compare their respective performance with that previously obtained with Pt/carbon xerogel samples prepared by another method with the same carbon support. The reference sample, denoted 'X-ref' hereafter corresponds to sample X2-Pt in a previous study [5]. This reference catalyst was synthesized by impregnation with H_2PtCl_6 followed by direct reduction in liquid phase with $NaBH_4$, and the solution concentration was chosen so as to deposit 35 wt.% of Pt onto the support in one single impregnation step [17]. The double-impregnated catalyst reduced either at 200 °C (X-Pt-2) or at 450 °C (X-Pt-2/450), was used to prepare 50 cm^2 MEAs, which were further tested on a unit cell-test bench. The MEA preparation method, the test device and the measurement procedure are completely described in Ref. [5]. Briefly, the MEAs were prepared by the decal method [4,5], which consists of spraying an ink composed of Pt/carbon catalyst, water and ionomer (Nafion®) onto a support, *i.e.* a Kapton® sheet; afterwards, the electrolyte, *i.e.* a Nafion® membrane, and the commercial anode, are piled up on the sprayed layer. The commercial anodes used here were made from Pt-doped carbon black (40 wt.%) prepared by Tanaka Kikinzoku Kogyo (TKK) deposited by Paxitech onto a carbon felt (Gas Diffusion Layer GDL 2315 I6 with PTFE treatment from Freudenberg GmbH) with 0.6 mg_{Pt}/cm^2 platinum loading mixed with Nafion (0.24 $mg_{Nafion®}/cm^2$, *i.e.* Nafion®/Carbon = 0.36). The whole assembly is then hot-pressed, yielding the MEA. For sake of comparing our results, the catalytic layer thickness of the cathode was kept identical to that used with the reference material (sample X2-Pt, prepared on the same support, see [5]) by keeping constant the carbon mass in the catalytic layer. The Nafion®/carbon mass ratio of the ink used to prepare the MEAs, *N*/*C*, was fixed at 0.5.

After a standardized start-up procedure, polarization curves, *i.e.* the $U_{cell} = f(j)$ curves (where U_{cell} is the cell potential and j is the current density), were measured by setting the cell voltage at each desired value for 15 min, which assured the stabilization of the current intensity. Since catalysts X-Pt-2 and X-Pt-2/450 contain less platinum than the samples synthesized previously (15 wt.% instead of 30–35 wt.%, see below), the current was normalized with either the geometric area of the electrode (j_s) or the Pt metal loading of the cathode (j_m).

2.4. Electrochemical characterization of the catalysts

The electrochemically active Pt surface area of the double-impregnated catalyst, reduced either at 200 °C (X-Pt-2) or at 450 °C (X-Pt-2/450), was determined by CO stripping on a rotating disk electrode (EDT 101, Tacussel). The experiments were carried out on a thin active layer (AL) of Pt/C catalyst deposited onto a glassy carbon electrode. The AL was prepared from a suspension blended from 23.3 mg of catalyst, 466 mg of 5 wt.% Nafion® in alcohol (Aldrich), and 0.7548 mL of ultrapure water (18.2 MΩ cm, 3 ppb total organic compounds, Millipore Elix + Gradient). After homogenization in an ultrasonic bath for 1 h, 10 μL of the suspension was deposited on the electrode. This electrode (diameter = 5 mm) had been previously polished with diamond paste down to 10 μm and washed for 15 min in three successive ultrasonic baths of acetone, ethanol–water (1:1) and water. The suspension deposited was then dried and sintered for 15 min at 150 °C in air to reconstitute the Nafion® and to ensure the binding of the AL to the glassy carbon surface. In order to remove the air contained in the AL and to fill its porosity with electrolyte solution, a drop of H_2SO_4 1 M was deposited onto the catalyst, prior to outgassing under vacuum until no air bubbles were visible.

CO stripping measurements were carried out in sulphuric acid (1 M, Suprapur-Merck) at 25 °C, using an Autolab-PGSTAT20 potentiostat with a three-electrode cell and a saturated calomel electrode (SCE) as reference (+0.245 V *vs.* normal hydrogen electrode, NHE). However, all the potentials are expressed on the NHE scale hereafter. The Pt surface was saturated with CO (N47, Alphagaz) by bubbling for 6 min in the solution; afterwards, the non-adsorbed CO was removed from the cell by Ar bubbling for 39 min. During the CO adsorption and Ar bubbling, the electrode potential was held at +0.095 V *vs.* NHE. Voltammetric cycles were then recorded at 0.02 V s^{-1} between +0.045 and +1.245 V *vs.* NHE. The active area of platinum, $S_{CO\text{-}strip}$, was calculated assuming that the electrooxidation of a full monolayer of CO_{ads} requires 420×10^{-6} C cm_{Pt}^{-2} [18].

3. Results

3.1. Physico-chemical characterization of the support and catalysts

The textural parameters of the carbon support chosen to prepare the catalysts are shown in Table 1. The carbon xerogel is a micro-macroporous material with a relatively high specific surface area (643 $m^2 g^{-1}$), and a macropore size ranging from 50 to 85 nm. Table 1 also shows the textural parameters of the support measured after successive impregnation steps. It must be noted that each parameter was corrected so as to take into account the mass increase due to metal addition to the porous support. In other words, all parameters are expressed per mass unit of carbon, not of catalyst. These results show that the pore texture of the support does not change much after one, two or three successive impregnations. The specific surface area of the carbon decreases slightly, from 643 $m^2 g^{-1}$ (raw support) to 526 $m^2 g^{-1}$ (X-Pt-3), which is probably due to partial blocking of the micropores by the metal particles.

Table 2
Catalyst characterization results.

Catalyst	ICP-AES	TEM				XRD	CO chemisorption				CO stripping	XPS
	Pt_{ICP} (wt.%)	d_{TEM} (nm)	σ (nm)	d_s (nm)	d_v (nm)	d_{XRD} (nm)	$n_{s,m}$ (mmol g_{Pt}^{-1})	D_{Pt} (%)	d_{CO} (nm)	$S_{CO\text{-}chem}$ (m^2 g_{Pt}^{-1})	$S_{CO\text{-}strip}$ (m^2 g_{Pt}^{-1})	Cl/Pt (–)
	±0.1	±0.2				±0.2	±0.05	±2	±0.2	±4	±10%	±0.05
X-Pt-1	7.5	2.0	0.7	2.5	2.7	2.6	1.15	36	3.1	92	–[a]	–[a]
X-Pt-2	15.0	1.9	0.8	2.5	2.8	2.6	1.10	34	3.2	89	37	0.33
X-Pt-3	22.7	2.0	0.7	2.6	2.8	2.7	1.11	35	3.2	89	–[a]	–[a]
X-Pt-2/450	15.0	2.0	0.7	2.5	2.7	2.7	1.53	48	2.3	124	127	0.07
X-ref [5]	31.0	–[b]	–[b]	–[b]	–[b]	–[b]	0.82	16	6.9	41	32	0.05

Pt_{ICP} = Pt weight percentage of the catalyst measured by ICP-AES; d_{TEM} = average particle size estimated from TEM; σ = standard deviation associated with d_{TEM}; d_s = average surface diameter of Pt particles, $\sum n_i d_i^3 / n_i d_i^2$, estimated from TEM; d_v = mean volume diameter of metal particles, $\sum n_i d_i^4 / n_i d_i^3$, estimated from TEM; d_{XRD} = average size of Pt particles estimated from X-ray peak broadening; $n_{s,m}$ = amount of CO needed to form a chemisorbed monolayer on surface Pd atoms; D_{Pt} = metal dispersion; d_{CO} = equivalent average Pt particle diameter obtained from CO chemisorption; $S_{CO\text{-}chem}$ = accessible Pt surface deduced from CO chemisorption; $S_{CO\text{-}strip}$ = accessible Pt surface deduced from CO stripping; *Cl/Pt* = chlorine to platinum surface atomic ratio determined by XPS.

[a] Not measured.

[b] Not pertinent (bidisperse catalyst).

Elemental analysis (ICP-AES) provided the Pt weight percentage, Pt_{ICP}, of each catalyst (Table 2). ICP data show that Pt_{ICP} increases quite regularly with the number of impregnation cycles: indeed, it equals 7.5, 15.0 and 22.7 wt.% for X-Pt-1, X-Pt-2 and X-Pt-3, respectively. Fig. 1 presents TEM micrographs of samples X-Pt-1 and X-Pt-3. These pictures show that both catalysts are well dispersed and present an extremely low degree of agglomeration; the particles are homogeneous in size and shape. Both samples contain Pt particles *ca.* 2 nm in diameter, the number of which increases with the Pt weight percentage while keeping the same metal dispersion. Fig. 2 shows the particle size distributions of the three catalysts obtained by image analysis of TEM micrographs. In each case, the particle size ranges from 1 to 5 nm, and no significant statistical difference is detected in the size distributions: the average particle size, d_{TEM}, and the standard deviation of the distribution, σ, are equivalent for the three catalysts (1.9–2.0 and 0.7–0.8, respectively). XRD results confirm the good metal dispersion (Fig. 3: no narrow peak visible): the average diameter estimated by Scherrer's equation [16], d_{XRD} ranges from 2.6 to 2.7 nm. Since XRD is sensitive to the volume of the particles, the diameter estimated from Scherrer's equation corresponds to a volume weighted average diameter, $d_v = \sum n_i d_i^4 / n_i d_i^3$ [16], where n_i is the number of particles of diameter d_i. This latter parameter, estimated from particle size distributions obtained from TEM micrographs, matches well with d_{XRD}, whatever the catalyst (Table 2). It also asserts that the TEM pictures were representative of the catalyst morphology, and confirms the homogeneity of the three catalysts (Fig. 2).

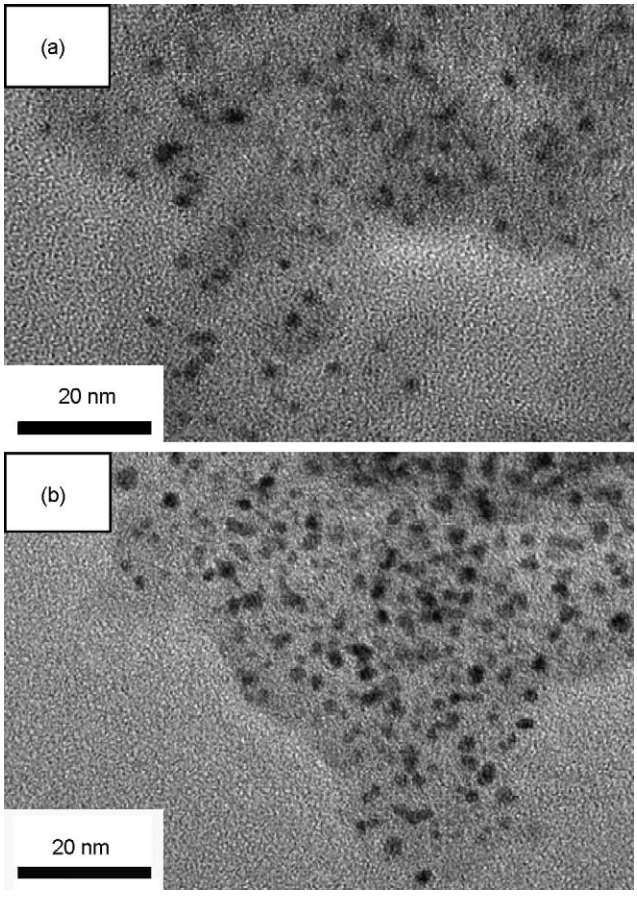

Fig. 1. TEM micrographs of the catalysts: (a) after one impregnation (X-Pt-1) and (b) after three successive impregnations (X-Pt-3).

The accessible surface of Pt was estimated from CO chemisorption measurements. The proportion of metal located at the surface of the Pt particles, *i.e.* the dispersion D_{Pt}, was calculated from [16]:

$$D_{Pt} = n_{s,m} M_{Pt} X_{Pt-CO} \times 10^{-3} \quad (2)$$

where $n_{s,m}$ is the amount of CO needed to form a chemisorbed monolayer on surface Pt atoms (mmol g_{Pt}^{-1}) and M_{Pt} is the atomic weight of Pt (195.09 g mol^{-1}). X_{Pt-CO} represents the chemisorption mean stoichiometry, *i.e.* the average number of Pt atoms on which one CO molecule is adsorbed. In the present study, X_{Pt-CO} was chosen equal to 1.61, following the results obtained by Rodríguez-Reinoso et al. in the case of Pt particles smaller than 5 nm [19]. The metal dispersion is nearly identical for X-Pt-1, X-Pt-2 and X-Pt-3: from 34 to 36%. An 'average equivalent particle diameter', d_{CO}, *i.e.* the particle diameter leading to a metal surface equivalent to that detected by chemisorption, is obtained by [16]:

$$d_{CO} = \frac{6(v_m/a_m)}{D_{Pt}} \quad (3)$$

where v_m is the mean volume occupied by a metal atom in the bulk of a metal particle (for Pt: v_m = 0.0151 nm^3) and a_m is the mean surface area occupied by a surface metal atom (for Pt: a_m = 0.0807 nm^2) [16]. The obtained average equivalent diameters range from 3.1 to 3.2 nm, and should be compared to a surface weighted average diameter, $d_s = \sum n_i d_i^3 / n_i d_i^2$ [16]. However, the particle size obtained by CO chemisorption, d_{CO} (3.1–3.2 nm), are systematically larger than those of the surface weighted average diameter d_s (2.5–2.6 nm), obtained from image analysis of TEM micrographs. Finally, the total

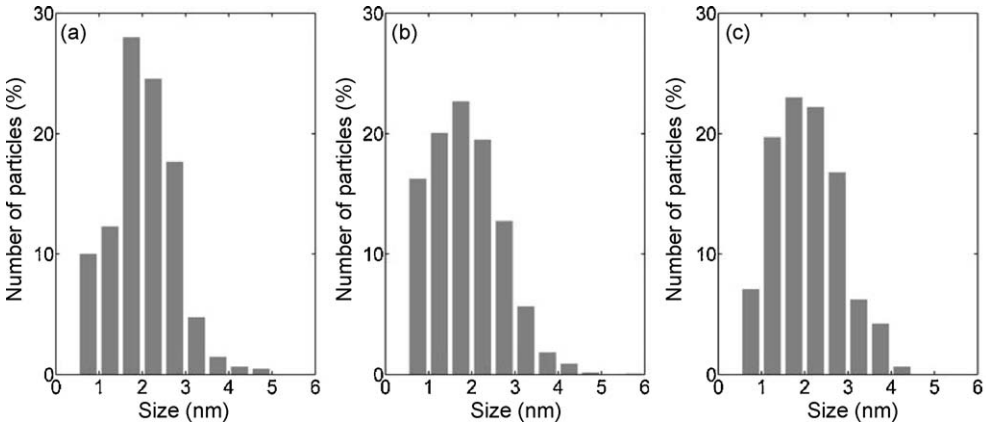

Fig. 2. Pt particle size distributions of the Pt/carbon xerogel catalyst issued from image analysis of TEM micrographs: (a) X-Pt-1, (b) X-Pt-2 and (c) X-Pt-3.

surface of the Pt particles, $S_{CO\text{-}chem}$, can be calculated from d_{CO} and the density of platinum, ρ_{Pt} (21.09 g cm^{-3}). Indeed:

$$S_{CO\text{-}chem} = 6\frac{V_{Pt}}{d_{CO}m_{Pt}} = 6\frac{1}{d_{CO}\rho_{Pt}} \quad (4)$$

where V_{Pt} and m_{Pt}, are the volume and the mass of Pt present in the catalyst, respectively. For X-Pt-1, X-Pt-2 and X-Pt-3, $S_{CO\text{-}chem}$ ranges from 89 to 92 m^2 g_{Pt}^{-1}.

The fraction of the catalyst X-Pt-2 that was reduced under H_2 at higher temperature (450 °C, 5 h), *i.e.* sample X-Pt-2/450, was characterized by all the methods used previously for the other catalysts. Characterization results show that: (i) the support properties do not change in comparison with the X-Pt-2 sample; (ii) the particle size distribution (not shown), as well as the average Pt particle size, determined from both TEM micrographs and XRD, do not evolve with regard to that of X-Pt-2 (Table 2); (iii) the Pt surface detected by CO chemisorption is higher ($S_{CO\text{-}chem}$ = 124 m^2 g_{Pt}^{-1} *vs.* 89 m^2 g_{Pt}^{-1} in the case of X-Pt-2, Table 2); (iv) d_{CO} (2.3 nm) is quite comparable to d_s (2.5 nm). This indicates that the reduction treatment at higher temperature does not modify the Pt distribution on the support, but increases the amount of Pt atoms accessible to reactants.

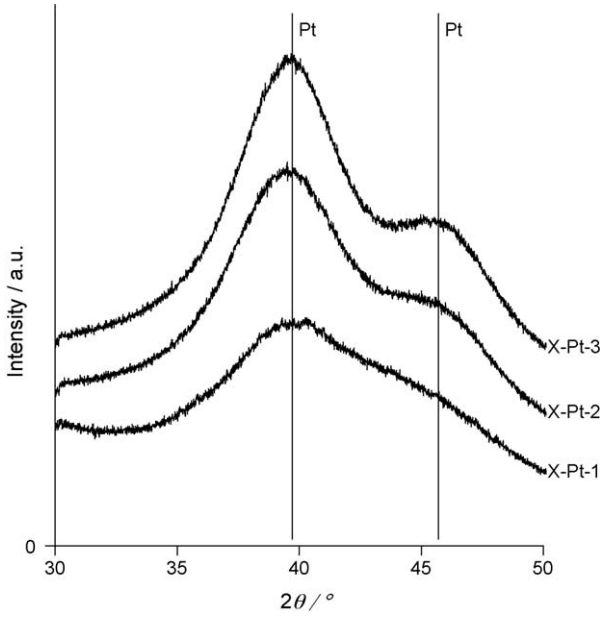

Fig. 3. X-ray diffractograms of the Pt/carbon xerogel catalysts after one, two and three successive impregnations.

The discrepancies between the Pt particle sizes obtained from TEM and CO chemisorption in the case of X-Pt-2, and between the CO surfaces obtained on X-Pt-2 and X-Pt-2/450, show that correlating the results obtained by both methods is not straightforward. Obviously, the two analysis methods do not match. The reasons for these discrepancies will be discussed in Section 4.

3.2. Fuel cell tests

Fig. 4 shows the polarization curve obtained with an MEA prepared with X-Pt-2 as cathodic catalytic layer. The MEA performance is compared to that of another MEA, processed from a Pt/carbon xerogel catalyst with a much lower metal dispersion, and prepared on the same carbon support. This reference sample is denoted 'X-ref' hereafter, and corresponds to sample X2-Pt in a previous study [5]. The reference catalyst, X-ref, was synthesized by impregnation with H_2PtCl_6 followed by direct reduction in liquid phase with $NaBH_4$, and the solution concentration was chosen so as to deposit about 35 wt.% of Pt onto the support in one single impregnation step [17]. During the reduction with $NaBH_4$ in aqueous phase, Pt ionic species adsorbed onto the support yield well-dispersed Pt particles [5,20] but forced reduction of platinum ions remaining in solution yields formation of large metal particles/aggregates on the carbon support. These mechanisms lead to a bimodal particle size distribution with two maxima located at *ca.* 2–5 and 10–30 nm. Hence, the catalyst displays a high Pt weight percentage (31.0 wt.%), but a poor dispersion (16%) and a low Pt surface area (41 m^2 g_{Pt}^{-1} [5,20]). Hence, X-Pt-2, the accessible Pt surface of which is much higher (89 m^2 g_{Pt}^{-1}) than that of X-ref, is expected to promote the oxygen reduction reaction at the cathode and to yield higher electrocatalytic performance.

However, Fig. 4 shows that the current density of the MEA containing catalyst X-Pt-2 at the cathode is dramatically lower than that of X-ref. Contrary to expected results, the increase in metal dispersion yields a decrease of the current density at U_{cell} = 0.4 V from j_s = 0.413 to j_s = 0.075 A cm^{-2} (Fig. 4a). Since the thickness of the catalytic layer is kept constant, and due to differences in metal weight percentage between X-ref (31.0 wt.%) and X-Pt-2 (15.0 wt.%), the metal loading of the two cathodes is not the same. The Pt loading of the cathodes, calculated by mass balance, amounts to 0.19 × 10^{-3} g_{Pt} cm^{-2} in the case of X-ref, and 0.10 × 10^{-3} g_{Pt} cm^{-2} in the case of X-Pt-2. Correcting the current production for the MEA metal loading (Fig. 4b) shows that the metal is about three times less active in the case of X-Pt-2: the current produced per mass unit of platinum, j_m, decreases from 2.09 to 0.68 kA g_{Pt}^{-1} at U_{cell} = 0.4 V.

By contrast, the polarization curve of the cell prepared with X-Pt-2/450 as cathodic catalyst is almost superimposed with that

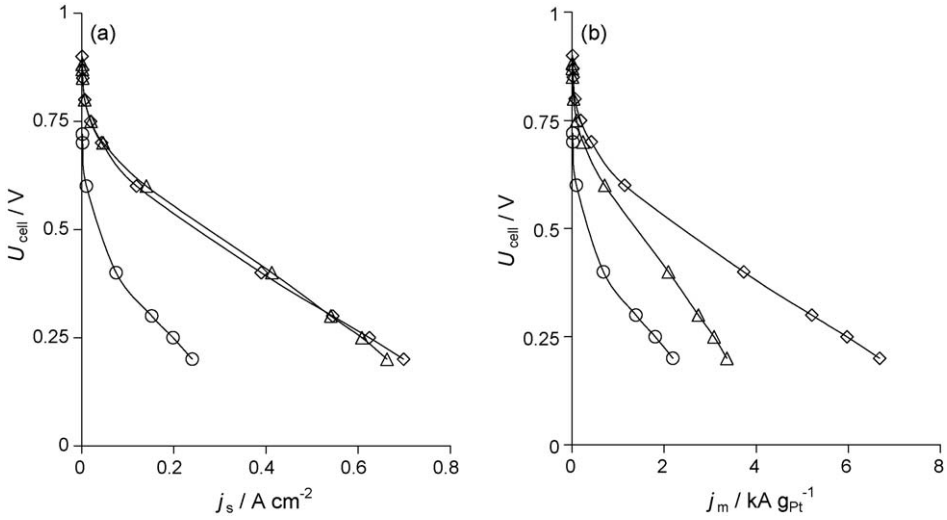

Fig. 4. Polarization curves at 70 °C for Membrane-Electrode Assemblies with cathode processed with (○) X-Pt-2, reduced at 200 °C (H_2, 1 h), (◇) X-Pt-2/450, reduced at 450 °C (H_2, 5 h) and (△) X-ref, *i.e.* catalyst prepared by impregnation with H_2PtCl_6 and reduced in liquid phase [5]. (a) Cell voltage *vs.* experimental current density per surface unit of electrode; (b) cell voltage *vs.* Pt mass activity.

obtained with X-ref when the current produced is expressed per cathode surface unit (Fig. 4a). Considering that the particle size distribution of X-Pt-2/450 and X-ref are similar in the small particles size domain, this agreement makes sense. Indeed, the largest particles (10–30 nm) present in X-ref represent a large fraction of the total mass of platinum loaded onto the carbon support but contribute very little to the electrochemically available surface area. On the other hand, normalization with the Pt loading of the cathode (0.10×10^{-3} g_{Pt} cm^{-2} in the case of X-Pt-2/450) leads to a much better MEA performance in terms of current produced per mass unit of Pt: j_m increases from 2.09 to 3.73 kA g_{Pt}^{-1} at U_{cell} = 0.4 V.

4. Discussion

As shown by Lambert et al. [11], the SEA of $PtCl_6^{2-}$ anions onto carbon xerogels leads to the preparation of very well dispersed Pt/C catalysts with a relatively high weight percentage (~8 wt.%). During the impregnation, the pH of the solution is adjusted so as to maximize the interaction of the Pt ions with the carbon surface, depending on the surface chemistry of the support. The $PtCl_6^{2-}$ species adsorb onto specific positively charged sites present onto the carbon support. The Pt uptake is limited by steric effects: indeed, the maximum surface density can be calculated as a close packed arrangement of chloroplatinic acid complexes which retain one hydration sheath [12]. Interestingly, the results from the present study show that these adsorption sites are completely recovered after the filtration, drying and reduction of the catalyst: as a consequence, consecutive impregnation steps lead to a regular increase in the Pt weight percentage. In addition, the recovered adsorption sites do not interact with the metal particles formed during the previous step: the number of deposited Pt particles increases without modifying the global metal dispersion. The size of the particles prepared after one, two or three successive impregnation cycles remains constant, which clearly shows that additional Pt particles are formed completely independently of the particles already present.

These results show that the SEA method is highly suitable for the preparation of highly dispersed Pt/C catalysts with low degree of agglomeration, although the impregnation procedure must be repeated to increase the metal weight percentage up to values acceptable for applications in PEM fuel cells. Carbon xerogels are very well adapted to this method: though their specific surface area, S_{BET}, is not extremely high in comparison with that of other carbon materials such as activated carbons or carbon blacks, it is possible to prepare metal nanoparticles with a high metal dispersion and homogeneous distribution onto the carbon support. The microporosity of the support is thus not a determining factor in the metal dispersion: the accessibility of the surface and its chemistry are the most important factors [11].

However, the catalytic performance of the obtained X-Pt-2 catalyst in PEM fuel cells cathodes is surprising. Despite a very high dispersion, the mass activity of X-Pt-2 is decreased with regard to sample X-ref, *i.e.* a catalyst composed of small (2–5 nm) and large (10–30 nm) Pt particles. This is particularly visible in Fig. 4a, for which the activation losses (*i.e.* obtained at low current density) amount to *ca.* 0.5 V for X-Pt-2 *vs. ca.* 0.25 V for the X-ref sample. Such higher activation losses could be due to several effects: (i) an improper particle size, (ii) the differences in electrode metal loading, (iii) a lack of contact between the Pt particles and the Nafion® network of the catalytic layer, (iv) the inaccessibility of the Pt particles to the gaseous reactants, or (v) the poisoning of the Pt particle surface by residues coming from the catalyst synthesis or even from the active layer elaboration procedure.

First, it is well known that the specific activity of Pt nanoparticles, *i.e.* the current produced per Pt surface area unit, strongly decreases with their size [13,21–23]. This has been related in the literature to the size dependence of the structure and electronic properties of metal nanoparticles, the so-called 'geometric' [22] and 'electronic effects' [24]. On the other hand, decreasing the Pt particle size yields an increase of specific surface area (cm^2 g_{Pt}^{-1}) which counterbalances the decrease of the specific activity. Hence, a maximum in mass activity (A g_{Pt}^{-1}) for the ORR has been reported at Pt particle sizes *ca.* 3–4 nm. In the present study, X-Pt-2 presents a higher dispersion than X-ref, which may explain partly the decrease in activity at low current densities. This cannot be confirmed by the sole comparison of X-Pt-2 and X-ref, and this issue will be discussed below.

Second, the difference in electrode metal loading (X-ref: 0.19×10^{-3} g_{Pt} cm^{-2}; X-Pt-2: 0.10×10^{-3} g_{Pt} cm^{-2}) may account for the observed differences at low and intermediate current densities. However, X-Pt-2 provides a higher accessible Pt surface area ($S_{CO\text{-}chem}$ = 89 m^2 g_{Pt}^{-1} *vs.* 41 m^2 g_{Pt}^{-1} in the case of X-ref [5]) and a simple calculation shows that comparable Pt surface areas are developed by both MEAs (X-Pt-2: 7.8×10^{-3} m_{Pt}^2 cm^{-2}; X-ref: 8.9×10^{-3} m_{Pt}^2 cm^{-2}).

Third, the lack of contact between Pt and Nafion® is also a well-known limitation of PEM fuel cells: only the Pt particles in contact with both the carbon support and the membrane, *via* a Nafion® network formed within the pore texture of the catalytic layer will be electrochemically active. Since the metal distribution, which can affect the Pt-Nafion® contact, is not the same in X-ref and X-Pt-2, one cannot draw direct conclusions. This will be discussed below.

Fourth, the catalytic sites must also be easily reachable by reactants. As illustrated by Thompson et al. [25], up to 90% of the platinum particles of a catalytic layer may be inactive, because of diffusional limitations in the catalytic layer or because most of the Pt particles are not in contact with the electrolyte (Nafion®); in both cases, the structure of the catalytic layer is the critical point. However, the macropore texture of the support was chosen so as to limit at best the diffusion overpotential of the cell [5], the Pt particles being mostly located outside the micropores, on the macropore surface [11]. Since the carbon chosen is the same in X-Pt-2 as in the case of the reference catalyst, X-ref, and since metal addition does not change the macropore size and volume (Table 1), diffusional limitations cannot account for the observed difference.

Finally, despite the reduction treatment at 200 °C in H_2 atmosphere, the presence of poisoning species at the surface of the Pt particles may explain the difference in activity between X-ref and X-Pt-2, the reduction treatment being quite different for the two catalysts. In particular, since H_2PtCl_6 was used as a metal precursor, chlorine is likely to poison the metal surface of Pt/carbon xerogel catalysts. Chlorine has already been suspected of partly covering the surface of the small metal particles present in the bidisperse Pt/carbon aerogel or Pt/carbon xerogel catalysts prepared in previous studies [5,20].

From direct electrochemical measurements on the MEAs, although activation losses are clearly observed for X-Pt-2, it is difficult to provide further insight into the origin of such limitations. Cyclic voltammetry provides the global metal active surface in the MEA but does not enable us to distinguish between the different hypotheses. By contrast, electrochemical characterization of the catalyst *via* CO stripping [26–28] provides interesting data. CO stripping involves the electrooxidation of a pre-adsorbed CO monolayer and does not require mass-transport in the electrolyte bulk. In addition, CO stripping experiments are usually performed in liquid electrolyte, which implies 100% utilization of Pt surface atoms and is not influenced by any contact problem between the metal and the electrolyte. The combination of the gas phase CO chemisorption and the electrochemical CO oxidation is also of great interest in unveiling the presence of poisons issued from the catalyst preparation. In this ambit, electrochemical characterization results of X-Pt-2 are compared with those of the reference catalyst, but also with data obtained after reduction of X-Pt-2 at higher temperature, *i.e.* X-Pt-2/450.

Fig. 5 shows the CO_{ads} voltammograms of the catalysts X-Pt-2, X-Pt-2/450 and X-ref. Note that, since the Pt weight percentage of the catalysts is not the same (X-ref: 31.0 wt.%, X-Pt-2 and X-Pt-2/450: 15.0 wt.%), and because the current measured is reported per mass unit of Pt, the signal corresponding to the support is lower for X-ref. CO_{ads} electrooxidation on Pt proceeds *via* a Langmuir–Hinshelwood mechanism, which includes water dissociation into oxygen-containing species, and recombination of the former species with CO, yielding CO_2 [26]. The electrooxidation of a CO_{ads} monolayer is a structure-sensitive reaction and provides a wealth of information on the particle size distribution and the presence/absence of particle agglomeration [26–28]. As detailed in a previous study [20], the reference catalyst, X-ref, presents three oxidation peaks centred at about +0.73, +0.81 and +0.92 V *vs*. NHE, corresponding to CO_{ads} electrooxidation at Pt particle agglomerates, large Pt particles ($d > 3.3$ nm) and small Pt nanoparticles ($d \sim 1.9$ nm), respectively. This agrees with TEM observations, which show that the particle size distribution of the catalyst is bimodal: large particles of a size *ca.* 10–30 nm and smaller particles *ca.* 2–5 nm.

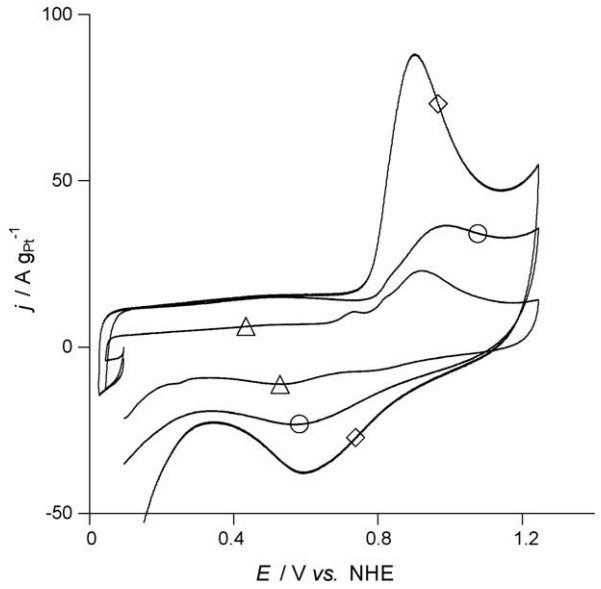

Fig. 5. CO_{ads} stripping voltammogram on the two catalysts in H_2SO_4 (1 M) at 25 °C; sweep rate of 0.02 V s^{-1}. (○) X-Pt-2, reduced at 200 °C (H_2, 1 h), (◇) X-Pt-2/450, reduced at 450 °C (H_2, 5 h) and (△) X-ref, *i.e.* catalyst prepared by impregnation with H_2PtCl_6 and reduced in liquid phase [5].

In the case of X-Pt-2/450, a main electrooxidation peak is observed at *ca.* +0.81 V *vs*. NHE (Fig. 5), indicating the presence of particles with a $d > 3.3$ nm. The current tailing at potentials more positive than the peak potential indicates the presence of smaller particles [26–28]. This parallels remarkably our previous TEM observation (see Fig. 2, the distribution of X-Pt-2/450 being the same as that of X-Pt-2). On X-Pt-2 the main electrooxidation peak is shifted towards positive potentials if one compares it to that of X-Pt-2/450. This trend is easily reproducible with a commercial 10 wt.% Pt/Vulcan XC72 (E-TEK) electrocatalyst with a similar Pt particle size (*ca.* 2.3 nm) in Cl-containing electrolyte. The positive shift of the onset of the CO electrooxidation peak may be ascribed to the competition between water and chloride species for the adsorption sites. Indeed, both experimental [28] and computational modelling studies [29] have suggested that there are only a fixed number of active sites on the Pt surface, which are able to form OH species and to initiate the CO electrooxidation. Competitive adsorption by Cl^- species will thus decrease artificially the number of active sites and shift both the onset and the main CO electrooxidation peak towards positive potentials. Experimental [26,28] and modelling studies [29] have also demonstrated the great importance of CO supply to these active sites. Therefore, any species competing for the same adsorption sites as CO will decrease its surface mobility (affecting the recombination of CO and oxygen-containing species) and increase the peak asymmetry at high electrode potentials. This is in line with the observed slow current decay observed for X-Pt-2/450 *vs*. X-Pt-2 at high electrode potentials.

The poisoning hypothesis is also supported by the comparison of Pt surface areas determined either by CO chemisorption or CO_{ads} stripping voltammetry (Table 2). Whereas $S_{CO\text{-}strip}$ and $S_{CO\text{-}chem}$ agree reasonably for X-ref (32 and 41 $m^2\ g_{Pt}^{-1}$ [5], respectively), a pronounced disagreement is observed for X-Pt-2 (37 and 89 $m^2\ g_{Pt}^{-1}$, respectively). This clearly shows that a large fraction of the surface of X-Pt-2 is not available from an electrochemical point of view, *i.e.* for the adsorption of CO or oxygen species in an

electrochemical environment. In addition, the CO_{ads} stripping voltammogram displays a much higher electrooxidation signal in the case of X-Pt-2/450 than in the case of X-Pt-2 (Fig. 5). The corresponding Pt surface area, $S_{CO\text{-}strip}$, equals 127 $m^2\ g_{Pt}^{-1}$, which now matches perfectly with $S_{CO\text{-}chem}$ = 124 $m^2\ g_{Pt}^{-1}$. Comparison between X-Pt-2 and X-Pt-2/450 indicates that a high reduction temperature is necessary to render the Pt surface accessible. Since electrochemical experiments in liquid electrolyte imply a 100% utilization of the Pt surface, this also discards the possible limitation of the MEA cathode through a lack of contact between Pt and Nafion® and reinforces the hypothesis that chlorine/chloride species coming from the Pt precursor (H_2PtCl_6) may poison the electrocatalytic activity by blocking some surface sites.

In order to confirm the presence of chlorine, XPS measurements were performed on catalysts X-Pt-2 and X-Pt-2/450. Chlorine was detected in both cases, but the Cl/Pt ratio, deduced from the relative surface of the Cl and Pt peaks, decreases from 0.33 to 0.07 when the reduction temperature increases from 200 to 450 °C. This confirms that a high temperature is required to eliminate chlorine originating from the Pt precursor, H_2PtCl_6. Note that, since Cl/Pt = 0.07 is close to the detection limit of the XPS device, one can suspect that 450 °C is not sufficient to completely remove chlorine. In addition, in the case of the reference catalyst X-ref, which underwent two reduction steps ($NaBH_4$ in aqueous media and H_2 at 350 °C) small amounts of chlorine are still detected Cl/Pt ∼ 0.05. As a general comment, chlorine compounds issued from the reduction of the platinum precursor are difficult to eliminate, and measurements on the single cell test bench show that small amounts of Cl can decrease dramatically the catalyst activity. This effect was already shown by Marceau et al. [30]: methane oxidation on Pt/γ-Al_2O_3 catalysts prepared by impregnation of alumina with H_2PtCl_6 was clearly inhibited by the presence of remaining chlorine compounds after reduction at 500 °C under H_2.

The difference in surface detected by CO chemisorption and CO stripping for sample X-Pt-2 (and, to a lesser extent, for X-ref) could be due to Cl displacement kinetics. Holscher and Sachtler [31] showed that CO is one of the strongest poisons adsorbed onto platinum: in the presence of CO, poisons originally adsorbed onto the Pt particle surface should be displaced. However, the kinetics of displacing may be too slow to be completed within a few minutes: this would explain why CO chemisorption in gaseous phase, during which equilibrium is reached prior to any further gas injection, leads to larger Pt surfaces than CO_{ads} stripping in liquid phase. It is interesting to note that neither CO stripping, nor CO chemisorption can displace completely the poisons: in both cases, the metal surface detected in X-Pt-2 is lower than that of X-Pt-2/450.

Finally, the polarization curve of the cell prepared with X-Pt-2/450 as cathodic catalyst shows that the performance of the cell now equals that obtained with the reference catalyst in terms of MEA specific current density, expressed per cathode surface unit (Fig. 4a): the polarization curves are almost superimposed on the whole range of cell voltage. This expresses the fact that the two catalysts exhibit: (i) the same activation losses, (ii) the same ohmic losses and (iii) the same diffusion losses. This naturally derives from the fact that the same membrane and the same assembling procedure were used in both cases. The morphology of the cathode active layer is maintained: the cathodes were prepared at constant thickness, regardless of the Pt particle morphology. Normalizing the results by the cathode Pt loading shows that the metal is better used in the case of X-Pt-2/450: indeed, the activity of X-Pt-2/450 is superior to that of X-ref, and of course to that of X-Pt-2 (Fig. 4b). This last result rules out any hindrance by an inappropriate particle size in the case of X-Pt-2: indeed, sample X-Pt-2/450 exhibits the same Pt particle size distribution as X-Pt-2, and a much higher activity than the MEA cathodic catalyst.

5. Conclusions

This study demonstrates that the SEA method allows the fine control of the structure and the morphology of the metal nanoparticles (average particle size, size distribution, degree of agglomeration) and it may thus be used to minimize the mass of Pt used in PEM fuel cells.

Pt/carbon xerogel catalysts with high metal weight percentages (up to 22.5 wt.%) were successfully prepared by successive impregnations with H_2PtCl_6 in 'Strong Electrostatic Adsorption' (SEA) conditions. Three successive steps were necessary to achieve this metal weight percentage, but characterization shows that the metal dispersion is not altered by the successive impregnation–drying–reduction cycles: the density of Pt particles on the carbon support increases, but their size remains nearly constant (∼2 nm). The final reduction conditions proved to be critical in the catalyst synthesis process. Indeed, catalysts reduced at 200 °C (H_2, 1 h) showed a poorly accessible Pt surface area and a low performance as cathodic catalysts in a Proton Exchange Membrane (PEM) fuel cell, most likely because of Pt poisoning by residues issued from the synthesis procedure. By contrast, increasing the reduction temperature and duration up to 450 °C and 5 h, respectively, led to a significant increase in the Membrane-Electrode Assembly (MEA) performance: this is attributed to the development of the active Pt surface area, both in the catalyst and in the cathode of the MEA.

The presence of chlorine, originating from $PtCl_6^{2-}$ decomposition and suspected to poison the Pt catalysts, was confirmed by XPS measurements. The effect of chlorine on the intrinsic activity of the catalyst is still under investigation. The replacement of H_2PtCl_6 by another Pt precursor in the SEA method is also envisaged in future studies.

Acknowledgements

N.J., S.L. and C.J.G. are postdoctoral researchers of the F.R.S.-FNRS (Belgium). The Belgian authors thank the Fonds de Recherche Fondamentale Collective, the Ministère de la Région Wallonne and the Interuniversity Attraction Pole (IAP-P6/17) for their financial support, and acknowledge the involvement of their laboratory in the Network of Excellence FAME of the European Union Sixth Framework Programme. The French authors thank the Groupement des Écoles des Mines (GEM). N.J. and M.C. thank Egide and the WBI for funding within the Hubert Currien partnership (project Tournesol #20389PF).

Appendix A

A.1. Image analysis algorithm used for the estimation of particle size distribution

The image analysis procedure used to determine the size distribution of the metal particles from the TEM micrographs is summarized in Fig. 6. The noise that is initially present in the original micrograph is first reduced by applying a low-pass Gaussian filter (Fig. 6a to b) [32]. In the obtained image, the particles are present as dark objects; they can be highlighted using a morphological operation called a negative top-hat [33], which is sensitive to local minima in images (Fig. 6c). The obtained image is then binarized using Otsu's method, *i.e.* by choosing the threshold that maximizes the between-class variance of the histogram of grey-levels [34].

The obtained binary image contains two types of white object. One type of object corresponds to the metal particles. Objects of the second type are generally larger and with a more irregular shape; they correspond to the overlapping of several particles. The two types of object were discriminated automatically on the basis

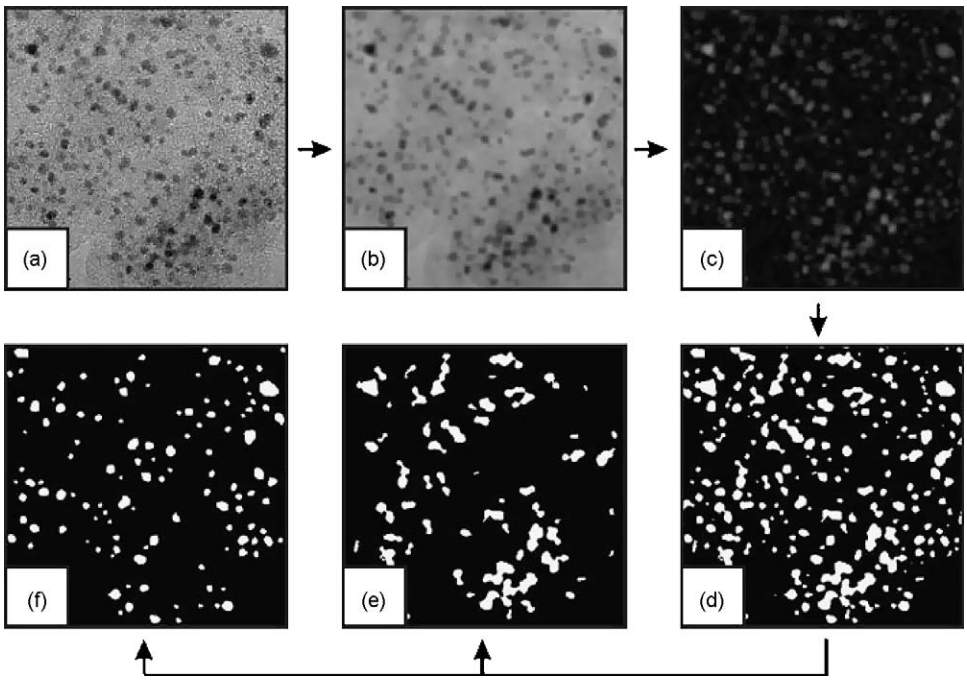

Fig. 6. Image analysis algorithm used to segment the metal particles and to obtain their size distribution. The initial micrographs (a) are first denoised applying a Gaussian filter (b); a negative top-hat transformation is applied to highlight the local minima (c), and the obtained image is segmented using Otsu's method (d). In the binary image many objects result from the overlapping of several particles; using morphological criteria, these can be discriminated from the isolated measurable particles (e and f, see text).

of their solidity and of their elongation, as explained below. The solidity of an object is defined as the ratio of its area to the area of its convex hull [32], *i.e.* the area of the smallest convex object that can contain it. For instance, the solidity of a disk is 1, whereas the solidity of a U-shaped object is significantly smaller than 1, as most of the area of its convex hull would correspond to the empty central part of the U. As for the elongation, this is defined as the ratio of the lengths of the two axes of an ellipse having the same moments as the considered object. The elongation of a disk is 1, and the elongation of any object larger in one direction than in the other is larger than 1. In the present case, particles can be isolated in the binary image as the objects with a solidity larger than 0.9, and an elongation smaller than 1.5. Applying these two criteria enables us to discriminate between particles (Fig. 6f) and other objects (Fig. 6e).

The size of every metal particle in the final image (Fig. 6f) is determined as the diameter of the disk having the same number of pixels as the segmented white object. As the criteria used to discriminate between particles and other objects are not sensitive to the size of the objects, this is an unbiased estimator of the actual size of the metal particles. On average, about 1000 particles are measured to determine the size distribution of each sample.

Appendix B. Supplementary data

Supplementary data associated with this article can be found, in the online version, at doi:10.1016/j.cattod.2009.06.022.

References

[1] H.A. Gasteiger, W. Gu, R. Makharia, M.F. Mathias, B. Sompalli, in: W. Vielstich, A. Lamm, H.A. Gasteiger (Eds.), Handbook of Fuel Cells—Fundamentals Technology and Applications, vol. 3, Wiley, Chichester (UK), 2003, p. 593.
[2] H.P. Boehm, Z. Anorg. Allg. Chem. 297 (1958) 315.
[3] H.A. Gasteiger, S.S. Kocha, B. Sompalli, F.T. Wagner, Appl. Catal. B 56 (2005) 9.
[4] J. Marie, S. Berthon-Fabry, M. Chatenet, E. Chainet, R. Pirard, N. Cornet, P. Achard, J. Appl. Electrochem. 37 (2007) 147.
[5] N. Job, J. Marie, S. Lambert, S. Berthon-Fabry, P. Achard, Energy Convers. Manage. 49 (2008) 2461.
[6] J. Marie, R. Chenitz, M. Chatenet, S. Berthon-Fabry, N. Cornet, P. Achard, J.Power Sources 190 (2009) 423.
[7] R.W. Pekala, J. Mater. Sci. 24 (1989) 3221.
[8] S.A. Al-Muhtaseb, J.A. Ritter, Adv. Mater. 15 (2003) 101.
[9] N. Job, A. Théry, R. Pirard, J. Marien, L. Kocon, J.-N. Rouzaud, F. Béguin, J.-P. Pirard, Carbon 43 (2005) 2481.
[10] N. Job, B. Heinrichs, S. Lambert, J.-P. Pirard, J.-F. Colomer, B. Vertruyen, J. Marien, AIChE J. 52 (2006) 2663.
[11] S. Lambert, N. Job, L. D'Souza, M.F.R. Pereira, R. Pirard, B. Heinrichs, J.L. Figueiredo, J.-P. Pirard, J.R. Regalbuto, J. Catal. 261 (2009) 23.
[12] J.R. Regalbuto, in: J.R. Regalbuto (Ed.), Catalyst Preparation: Science and Engineering, CRC Press, Taylor & Francis Group, Boca Raton, 2007, p. 297.
[13] K. Kinoshita, Electrochemical Oxygen Technology, Wiley, New York, 1992, p. 48.
[14] C. Alié, R. Pirard, A.J. Lecloux, J.-P. Pirard, J. Non-Cryst. Solids 246 (1999) 216.
[15] N. Job, M.F.R. Pereira, S. Lambert, A. Cabiac, G. Delahay, J.-F. Colomer, J. Marien, J.L. Figueiredo, J.-P. Pirard, J. Catal. 240 (2006) 160.
[16] G. Bergeret, P. Gallezot, in: G. Ertl, H. Knözinger, J. Weitkamp (Eds.), Handbook of Heterogeneous Catalysis, Wiley–VCH, Weinheim, 1997, pp. 439–464.
[17] J. Marie, S. Berthon-Fabry, P. Achard, M. Chatenet, A. Pradourat, E. Chainet, J. Non-Cryst. Solids 350 (2004) 88.
[18] S. Trasatti, J. Electroanal. Chem. 327 (1992) 353.
[19] F. Rodríguez-Reinoso, I. Rodríguez-Ramos, C. Moreno-Castilla, A. Guerrero-Ruiz, J.D. López-González, J. Catal. 99 (1986) 171.
[20] N. Job, F. Maillard, J. Marie, S. Berthon-Fabry, J.-P. Pirard, M. Chatenet, J. Mater. Sci., doi: 10.1007/s10853-009-3581-x.
[21] K. Kinoshita, Carbon—Electrochemical and Physicochemical Properties, Wiley, New York, 1988, p. 48.
[22] K. Kinoshita, J. Electrochem. Soc. 137 (1990) 845.
[23] F. Maillard, S. Pronkin, E.R. Savinova, in: W. Vielstich, H.A. Gasteiger, H. Yokokawa (Eds.), Handbook of Fuel Cells, vol. 5, Wiley, New York, (2009) pp. 91–111.
[24] C.R. Henry, Surf. Sci. 31 (1998) 235.
[25] S.D. Thompson, L.R. Jordan, M. Forsyth, Electrochim. Acta 46 (2001) 1657.
[26] F. Maillard, M. Eikerling, O.V. Cherstiouk, S. Schreier, E. Savinova, U. Stimming, Faraday Discuss. 125 (2004) 357.
[27] F. Maillard, S. Schreier, M. Hanzlik, E.R. Savinova, S. Weinkauf, U. Stimming, Phys. Chem. Chem. Phys. 7 (2005) 385.
[28] F. Maillard, E.R. Savinova, U. Stimming, J. Electroanal. Chem. 599 (2007) 221.
[29] B. Andreaus, F. Maillard, J. Kocylo, E.R. Savinova, M. Eikerling, J. Phys. Chem. B 110 (2006) 21028.
[30] E. Marceau, H. Lauron-Pernot, M. Che, J. Catal. 197 (2001) 394.
[31] H.H. Holscher, W.M.H. Sachtler, Discuss. Faraday Soc. 41 (1966) 29.
[32] J.C. Russ, The Image Processing Handbook, CRC Press, Boca Raton (FL), 2002.
[33] P. Soille, Morphological Image Analysis: Principles and Applications, Springer, Berlin, 1999.
[34] N. Otsu, IEEE Trans. Syst. Man Cybern. 9 (1979) 62.